ARCHIVES OF ELECTRICAL ENGINEERING VOL. 72(3), pp. 697–713 (2023)

DOI 10.24425/aee.2023.146045

Investigation of local properties of the Fe-Si alloy subjected to mechanical and laser cutting

ZBIGNIEW GMYREK [1] ✉, BARBARA KUCHARSKA [2]

[1] *Institute of Mechatronics and Information Systems, Lodz University of Technology*
Stefanowskiego 22, 90-537 Łódź, Poland

[2] *Department of Materials Engineering, Czestochowa University of Technology*
Al. Armii Krajowej 19, 42-201 Częstochowa, Poland

e-mail: ✉*zbigniew.gmyrek@p.lodz.pl, barbara.kucharska@pcz.pl*

(Received: 05.02.2023, revised: 14.04.2023)

Abstract: The effective design of energy-saving electric motors with efficiency class IE4 and higher requires the use of material characteristics that take into account the core shaping process. Therefore, it becomes necessary to use analytical or numerical models that take into account the change of local properties of Fe-Si material. The aim of the work is to indicate a useful analytical model for estimating the local magnetic permeability of the material, as well as to understand the reasons for these changes. For this purpose, low-loss ferromagnetic materials cut with a guillotine and a laser were tested. Rectangular samples, cut at an angle of 0 degrees in relation to the rolling direction, were subjected to macroscopic and microscopic examinations. Finally, the main reasons for changes in material characteristics for both cutting technologies were indicated. Therefore, the proposed model takes into account not only the cutting technology used, but also the current width of the tested strip, for which the material characteristics are to be determined. The parameters of the analytical model are determined on the basis of a limited number of measurements carried out on samples of a simple geometric shape.

Key words: ferromagnetic materials, mathematical modeling, non-invasive measurements, structure destruction

1. Introduction

The design and production of modern, energy-saving induction and synchronous electric motors with the IE4 efficiency class is currently a major challenge for designers [1]. The correct design of this type of motor, meeting the high requirements in terms of minimizing power

consumption, requires excellent knowledge of the material parameters of the core [2–6]. The use of catalog data of Fe-Si laminates in the design process has long been abandoned. Therefore, it is important to use material characteristics that take into account the technological processes changing the properties of the ferromagnetic material [7]. An example of this is the shaping of stator and rotor laminates or embedding the fabricated core into the electric motor housing. This problem is particularly important in the case of cores whose fragments, e.g. the teeth, are relatively small (several mm wide). Moreover, the cores of prototype models are shaped by laser cutting, instead of the mechanical punching used in mass production. This fact must be taken into account in the process of designing and preparing a new motor structure, which will be directed to mass production.

Literature is full of examples of research focused on studying the impact of the technological process on changes in the properties of ferromagnetic material used in the production of motor cores [8, 9]. Among them, there are works showing a significant impact of the punching process on a change in magnetic permeability, as well as material specific loss [10, 11]. The main idea of these works is to show changes in material properties based on macroscopic non-invasive measurements, made for strips of several widths (from a few mm to several dozen mm) [12]. The conducted research mainly concerns the impact of mechanical cutting, while there are relatively few deepened studies on the effect of laser cutting [12–15]. In addition, a small group of research on the estimation of local material properties can be identified, based on the results of macroscopic examinations [12, 16–18]. In turn, other researchers deal with the observations at the level of the internal structure of the material, showing its changes resulting from the cutting technology used [19–21]. Others focus only on the study of the impact of mechanical stresses (resulting, for example, from the embedding of the core in the housing) to a change in the properties of ferromagnetic material [22, 23]. In this case, the tests are carried out on strips subjected to mechanical stress, assuming a uniform distribution of stresses in the sample volume.

Based on the literature review, it should be stated that further research is needed. Their goal is to link the results of macroscopic study, tests conducted at the level of the material structure, with the results of the assessment of local properties of ferromagnetic material. The authors of this paper try to expand scientific knowledge in this area. The paper is divided into several sections. The second section describes the results of macroscopic tests conducted with the use of the Single Strip Tester (the tests concern mechanically and laser-cut material). The third section describes the mathematical model used for estimating magnetic permeability of the material. The fourth section contains the mathematical model used for the estimation of local magnetic permeability and the results of measurements at the structure level. The article ends with a short discussion and conclusions.

2. Macroscopic measurements of material properties with the use of the Single Strip Tester

The aim of the conducted research was to find the relationship between the results of macroscopic tests and results of research on the structure of materials, partially damaged as a result of cutting. The research was carried out for two commonly used materials M300-35 and M470-50. In order to examine the impact of structure damage on the change in the properties of the material

subjected to the cutting process, rectangular strips with a width of 4 to 60 mm were prepared for testing. In this case, the share of damaged material zones is variable. Such sample preparation then enabled the development of a mathematical model describing changes in local material properties. The measurements were performed using the MAG-8.1HT computer measuring system – Fig. 1. It is designed to measure the dynamic magnetic properties of single strips of electrical sheet in the JM300-60HT test circuit. The measuring yoke is adapted to measure strips with a width of 60 mm. In the case of narrower strips, the number of strips has been selected so as to maximally fill the available 60 mm width (for example, 15 strips of 4 mm width were tested simultaneously).

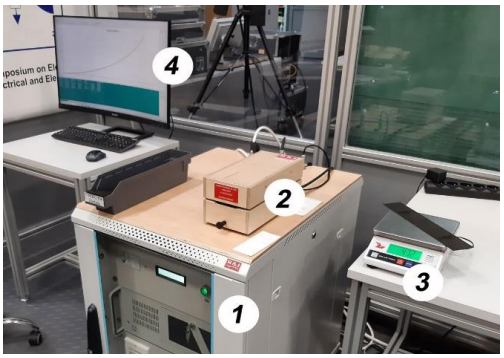

Fig. 1. Measurement stand: power electronic part of the measuring system – 1; measuring yoke – 2; scale and strip of the tested material – 3; monitor of the computer system – 4

The measurement of the magnetic field strength was carried out using the indirect method, and the average induction in the cross-section of the strip was determined on the basis of the voltage induced in the measuring coil placed on the test yoke. The excitation current and induced voltage curves were recorded. The specific loss of the tested material was determined from Formula (1)

$$p_s = \frac{1}{m_{\mathrm{Fe}}} \cdot \frac{z_1}{z_2} \cdot \frac{1}{T} \cdot \int_0^T u(t) \cdot i(t)\,\mathrm{d}t, \tag{1}$$

where: p_s is the specific loss of tested material, m_{Fe} is the weight of the test sample, z_1 and z_2 are the number of turns of the excitation winding and the number of turns of the coil measuring the induced voltage, respectively, T is the period of the excitation current and induced voltage waveforms, $u(t)$ and $i(t)$ are the waveforms of the induced voltage and the excitation current, respectively.

The measurement system used ensures the implementation of measurements in the range from 10 Hz to 4 kHz, with the frequency setting accuracy better than 0.1%. At the same time, the accuracy of mapping the sine waveform of induction in the tested sample is better than 1%, and the accuracy of determining material loss is better than 0.5%. In order to assess the effect of the cutting process on the change of material properties, the authors decided to test two commonly used materials. They have different thickness, different loss anisotropy and different chemical composition. The chemical composition and selected properties of these materials are included in Table 1. As the tested materials have loss anisotropy, strips cut at an angle of 0 degrees to the direction of rolling were tested. Two cutting technologies were used. The first technology used a guillotine with 3 m long knives and a maximum opening angle of 10 degrees. The knives

showed an average degree of wear, and the clearance between the blades reached 4% of the sheet thickness. The second technology used a 3 kW laser, with a nozzle height of 2.5 mm. Cutting was performed at a speed of 250 mm/s, in an compressed air environment, at a pressure of 0.8 MPa.

Table 1. Chemical composition of the tested materials (mass percent), average grain size and hardness

Material type	Fe	Si	C	Mn	Al	Average grain size (μm)	Hardness HV5
M300-35	96.7	2.5	0.003	0.27	0.39	150	220
M470-50	97.0	1.8	0.02	0.16	0.34	70	125

The tests were carried out at a frequency of 50 Hz. Sample measurement results of flux density vs. strip width curves and hysteresis loops are shown in Fig. 2, Fig. 3 and Fig. 4, respectively.

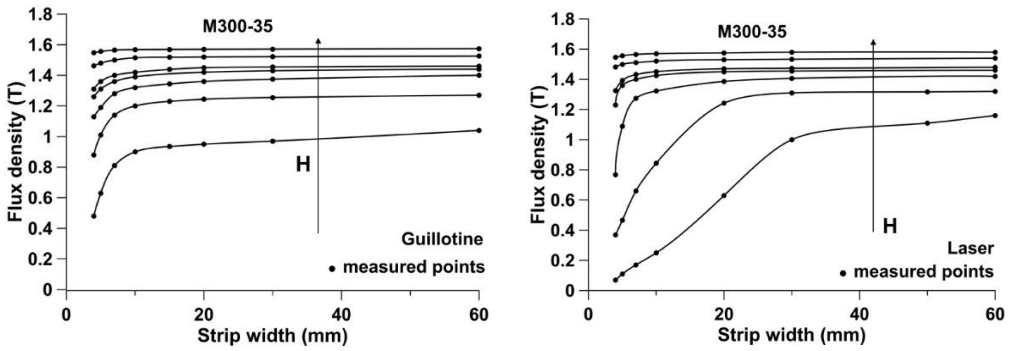

(a) (b)

Fig. 2. Measured curves of magnetic flux density vs. strip width (M300-35 material)

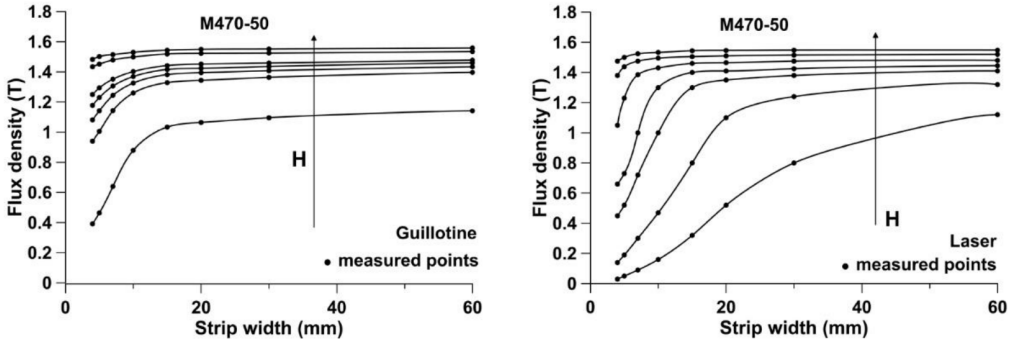

(a) (b)

Fig. 3. Measured curves of magnetic flux density vs. strip width (M470-50 material)

The flux density vs. strip width curves are plotted in a form that allows immediate identification of changes in material properties. The observed changes result from the different share of damaged material zones – the share depends on the current width of the strip. The letter H shown in the figures denotes the magnetic field strength for which the measurements were made, and the direction of its value increase. The results presented in the figures refer to the following magnetic field strengths (in A/m): 100, 250, 500, 800, 1 000, 2 000 and 3 000.

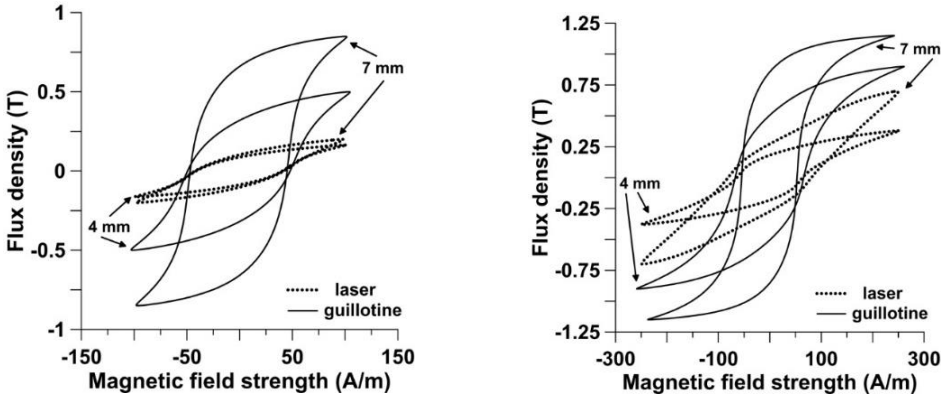

Fig. 4. Measured hysteresis loops for for strips of two widths (M300-35): H_{max} = 100 A/m (a); H_{max} = 250 A/m (b)

Depending on the applied cutting technology, different shapes of the coercive field curves as a function of the strip width were registered for both tested materials – Fig. 5. The results are presented for B_{ave} flux densities (averaged over a cross-section) of 0.1, 0.2, 0.4, 0.6 and 1 T, respectively.

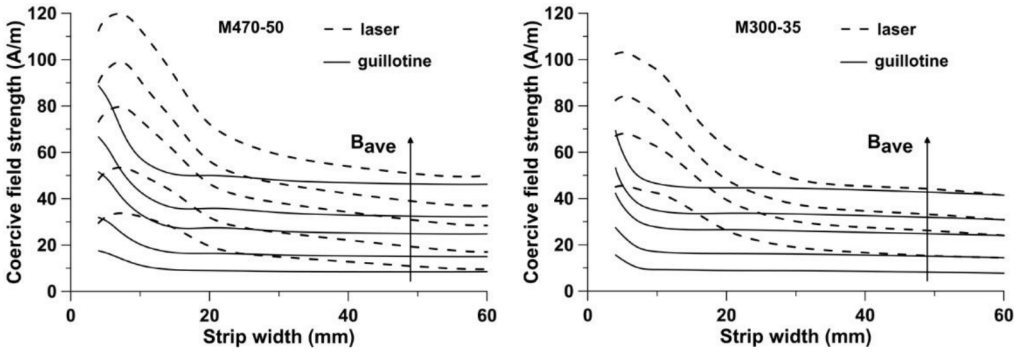

Fig. 5. The coercive field strength vs. strip width, measured at 50 Hz

Analyzing the results in Fig. 5, we find that the cutting process causes an increase in coercive field strength. For a specific induction, guillotine cutting causes an increase in coercive field strength for M470-50 strips with a width of less than 10 mm, while for M300-35 strips, an increase is observed only for widths smaller than 6 mm. The maximum increase in coercive field strength in relation to a strip of 60 mm width is: for M470-50 – about 100%, regardless of induction; for M300-35 – from 100% (for 0.1 T) to 70% (for 1 T). The situation with laser cutting is different. The width of the strip for which there is a noticeable increase reaches even 20 mm, while a rapid increase is registered for strip width below 12 mm. The maximum increase depends on the maximum induction and ranges from 140% (for 1 T) to 260% (for 0.1 T), regardless of the type of material. For strips with a width of less than 7 mm cut with a laser, there is a strong overlapping of the cutting effects of individual edges, which leads to a significant change in the properties of materials and is manifested by a decrease in coercive field strength.

3. Analytical model of changes in magnetic permeability of material cut by laser and guillotine

Analytical models describing changes in the material properties of the zones located at the cut edges can be found in the literature. In the available literature, there are several interesting papers that use this simple assumption [10, 24–27].

Based on the authors' own experience related to the construction of analytical models, the measurement results were presented in the form that is directly related to the change in relative magnetic permeability of the material (Fig. 2 and Fig. 3). Therefore, the flux density curves were determined for specific values of the magnetic field strength. Thus, after rescaling the y-axis values by the factor $1/H$ we obtain the values of $\mu_0\mu_r(x,H)$ magnetic permeability (averaged over cross-section of a strip) corresponding to a strip of a w certain width (where H is the magnetic field strength for which the measurement was made). As indicated in the available literature, the magnetic permeability change curves can be effectively approximated by exponential functions [10, 24–27]. Accepting the exponential nature of changes in magnetic permeability, the authors propose a modified relationship describing the change in magnetic permeability. The proposed relationship can be effectively used to approximate the measurement results of the average magnetic permeability (as a function of the strip width) and the local magnetic permeability (as a function of the distance from the cut edge). The proposed modification consists in adopting the $dd(x)$ exponent as dependent on the current strip width/distance from the cut edge (2).

$$\mu_r(x,H) = \mu_{rG}(H) + (\mu_{r00}(H) - \mu_{rG}(H))\, e^{-\frac{x}{dd(x)}}, \tag{2}$$

where: x is the current distance from the cut edge/current strip width, H is the magnetic field strength, $\mu_r(x,H)$ is the relative magnetic permeability of the material, at x distance/strip width and H magnetic field strength, $\mu_{rG}(H)$ is the relative magnetic permeability of the undamaged part of material, at H magnetic field strength, $\mu_{r00}(H)$ is the relative magnetic permeability of the material, at edge (must be found) and H magnetic field strength, $dd(x)$ is the characteristic distance, referred to in the literature as the "effective" width.

The local values of magnetic permeability, which change with the distance from the cut edge, are closely related to the measured average values of magnetic permeability. This results directly from the relationship between the measured average flux density (for a given width of the strip) and the unknown local flux densities for the elementary area located at a distance x from the edge.

$$B_{\text{ave}}(w,H) = \frac{1}{w}\int_0^w B_{\text{loc}}(x,H)\,\mathrm{d}x, \tag{3}$$

where $B_{\text{ave}}(w,H)$ is the measured average flux density for a strip of the w width and H magnetic field strength, w is the actual strip width, $B_{\text{loc}}(x,H)$ is the local flux density, at the x distance from the edge and H magnetic field strength.

Dividing both sides of Eq. (3) by $\mu_0 H$, we obtain

$$\mu_{r\text{ave}}(w,H) = \frac{1}{w}\int_0^w \mu_{r\text{loc}}(x,H)\,\mathrm{d}x, \tag{4}$$

where: $\mu_{r\text{ave}}(w,H)$ is the average magnetic permeability for a strip of the w width (e.g. $w = 10$ mm), μ_0 is the permeability of free space, w is the actual strip width, $\mu_{r\text{loc}}(x,H)$ is the local magnetic permeability.

4. Estimations and measurements of local material properties

4.1. Estimation of local magnetic permeability of a material

The macroscopic measurements described in Section 2 made it possible to determine the curves shown in Figs. 2 and 3. These curves obtained for the indicated magnetic field strengths are, therefore, identical to the curves representing the average magnetic permeability of the material. Hence, the first step was to find an approximation of the average relative magnetic permeability as a function of the strip width. For the specified H field strength, the following exponential approximations were used:

– approximation no. 1

$$\mu_{r\text{ave}}(w) = a + b\cdot\left(1 - e^{\left(-w\cdot\left(c+d\cdot\sqrt{w}\right)\right)}\right), \tag{5}$$

– approximation no. 2

$$\mu_{r\text{ave}}(w) = a + b\cdot\left(1 - e^{(-w\cdot c)}\right), \tag{6}$$

where a, b, c, d are the fitting parameters found in the error minimization process between the approximation and the measurement data, w is the strip width.

From the above it follows that the $dd(w)$ effective width is, respectively:

– $dd(w) = 1/(c + d\cdot\sqrt{w})$ for approximation no. 1,

– $dd(w) = 1/c$ for approximation no. 2.

Sample results for both materials, showing a significant improvement in the approximation accuracy especially for low magnetic field strengths, are shown in Table 2. Figure 6 shows the reconstructed curves of the average relative magnetic permeability, determined for the case of the highest approximation errors (for the magnetic field strength equal to 100 A/m).

Formula (3) shows an unambiguous relationship between the average and local magnetic flux density, and in the same way relationships between the average and local magnetic permeability (4). As shown above, very good results in approximating the average permeability were obtained using Formula (5) – see Table 2.

Table 2. Mean approximation error of the $\mu_{r\mathrm{ave}} = f(w)$ curves, using measurement data (in %)

Material type	**Guillotine**					
	Approx. no 1			Approx. no 2		
	2 000 A/m	800 A/m	100 A/m	2 000 A/m	800 A/m	100 A/m
M470-50	0.015	0.027	1.301	0.017	0.037	4.51
M300-35	0.001	0.025	0.062	0.004	0.059	1.21
	Laser					
M470-50	0.022	0.035	2.01	0.024	1.410	12.0
M300-35	0.002	0.060	1.20	0.008	0.122	17.1

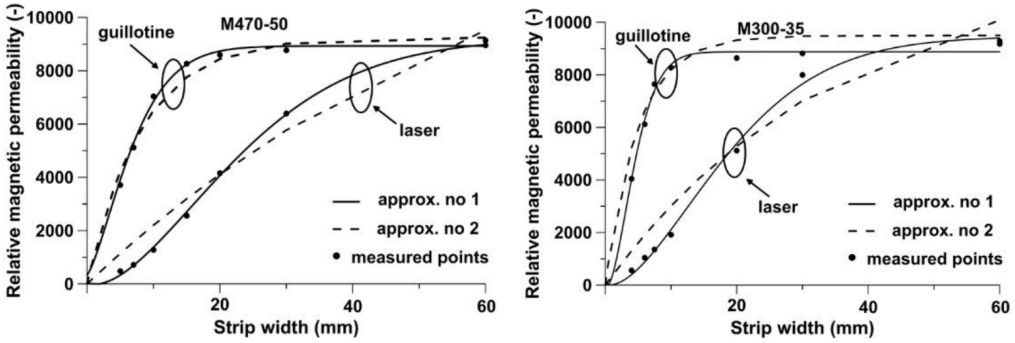

(a) (b)

Fig. 6. Reconstructed average relative magnetic permeability, at a field strength of 100 A/m

On the basis of the previously described activities, the fitting parameters of Formula (5) were determined. These parameters were determined for the given magnetic field strengths, for both types of tested materials, and for both cutting technologies. Then approximation (5) with known fitting parameters was used in Eq. (4). By performing numerical differentiation of Eq. (5), sets of points describing changes in local relative magnetic permeability were determined. In the next

step, the sets of points were approximated by the exponential function, (7), by determining its fitting parameters $a_1 \ldots e_1$.

$$\mu_{r\mathrm{loc}}(x, H) = a_1 + b_1 \cdot \left(1 - e^{(-x \cdot tt)}\right), \tag{7}$$

where: $\mu_{r\mathrm{loc}}(x, H)$ is the local relative magnetic permeability, tt is the characteristic parameter defined as $tt = c_1 + d_1 \cdot x + e_1 \cdot x^2$, a_1, b_1, c_1, d_1, e_1 are the fitting parameters, x is the actual distance from cut edge.

For Formula (7) the characteristic width $dd(x)$ is defined, with the known fitting parameters $a_1 \ldots e_1$ as $dd(x) = 1/\left(c_1 + d_1 \cdot x + e_1 \cdot x^2\right)$.

Approximation (7) maps with a certain accuracy a set of points obtained as a result of numerical differentiation. For each analyzed case, the coefficients a_1, b_1, c_1, d_1 and e_1 of the Eq. (7) were determined. Then the authors proceeded to the last step of the procedure, which was to insert Formula (7) into Eq. (4). Then, numerical integration was carried out and the obtained values of the average magnetic permeability were compared with those obtained from the measurements. The results of the comparison are presented in Table 3.

Table 3. Mean approximation error of the $\mu_{r\mathrm{ave}} = f(w)$ curves, using $\mu_{r\mathrm{loc}} = f(x)$ (in %)

Material type	**Guillotine**			**Laser**		
	2 000 A/m	800 A/m	100 A/m	2 000 A/m	800 A/m	100 A/m
M470-50	0.010	0.081	2.01	0.021	0.450	0.71
M300-35	0.008	0.011	0.44	0.012	0.110	0.91

An example comparison of the $\mu_{r\mathrm{ave}} = f(w)$ curves, determined using the $\mu_{r\mathrm{loc}} = f(x)$ curves, with the measurement data is shown in Fig. 7. While Fig. 8 shows the $dd(w)$ and $dd(x)$ curves obtained for approximations (5), (6) and (7).

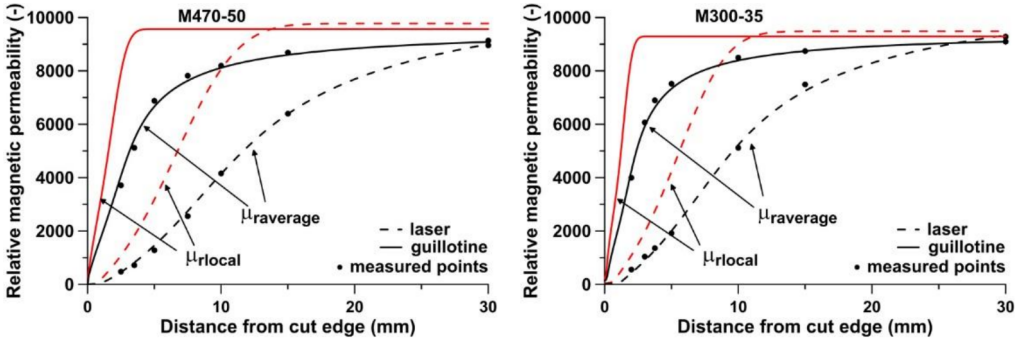

(a) (b)

Fig. 7. Reconstructed $\mu_{r\mathrm{ave}}$ and $\mu_{r\mathrm{loc}}$ curves, at a field strength of 100 A/m

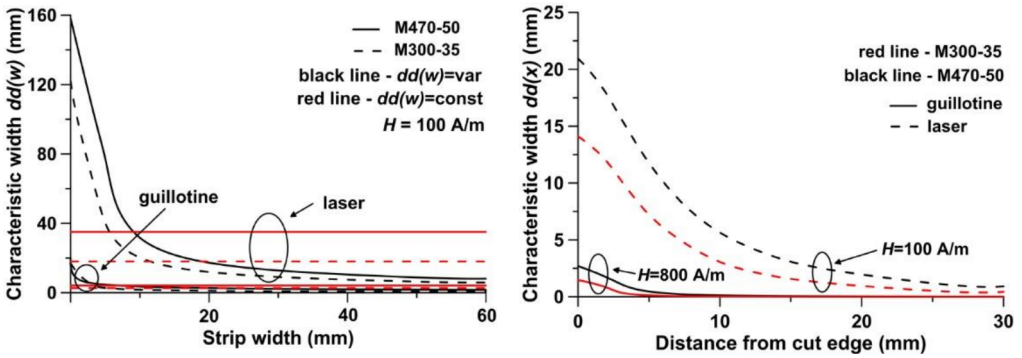

Fig. 8. Characteristic width $ddt(w)$ vs strip width (a), and characteristic width $dd(x)$ vs distance from cut edge (b)

4.2. Measurements of microhardness

As a result of microhardness and residual stress tests, the influence of the strip cutting method on their properties was determined. The microhardness was measured using the Vickers method (Shimadzu microhardness tester) using a diamond indenter. The assumed load F = 98 mN (0.01 kG) and the time of penetration of the indenter into the material equal to 10 s. Measurements were made on the surfaces of strips previously used in microstructure studies. In the central part of the strip, the average microhardness of the material was measured with a value of approx. 219 ± 20 HV0.01 (M300-35 material) and 123 ± 20 HV0.01 (M470-50 material). The results of microhardness measurements made at different distances from the cut edge are shown in Fig. 9.

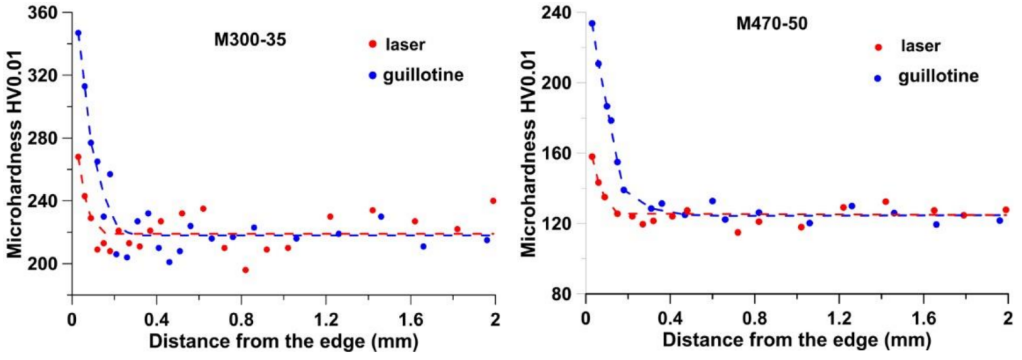

Fig. 9. The measured microhardness of the material vs. distance from the cut edge

In the case of the guillotine-cut strip, for the part of the material located at the edge, the microhardness was higher (due to strain hardening) than in the rest of the strip, reaching a maximum of 350 HV0.01 (for M300-35) and 236 HV0.01 (for M470-50). The width of the zone characterized

by greater hardness was about 200 µm (M300-35) and about 380 µm (M470-50), respectively, which is comparable to the zone of deformed microstructure. An increase in hardness up to 270 HV0.01 (M300-35) and 160 HV0.01 (M470-50), at the edge of the laser-cut strip, was also observed. This meant a smaller increase than a guillotine cut. In this case, the area of increased microhardness was estimated at about 70–80 µm (for both materials). At the same time, SEM tests conducted for M300-35 material, showed a smaller size of the remelting zone. It follows that the heat affected zone during laser cutting of the investigated M300-35 strip was approx. 20–30 µm (Fig. 11(c)).

4.3. Observations of the grain structure

The metallographic preparation revealed the microstructure of the strip material in the areas at the cut edge. For this purpose, the strips were cut in two planes: parallel to the strip surface and in a plane perpendicular to the strip surface. The surfaces of the tested strips were ground with polishing cloths containing a diamond suspension (particles 3 and 1 µm) using a Buehler metallographic polisher. Polished surfaces were etched with an aqueous solution of nitric and hydrochloric acid. The revealed microstructures of the strips, observed with the VHX-7 000 microscope, are shown in Fig. 10.

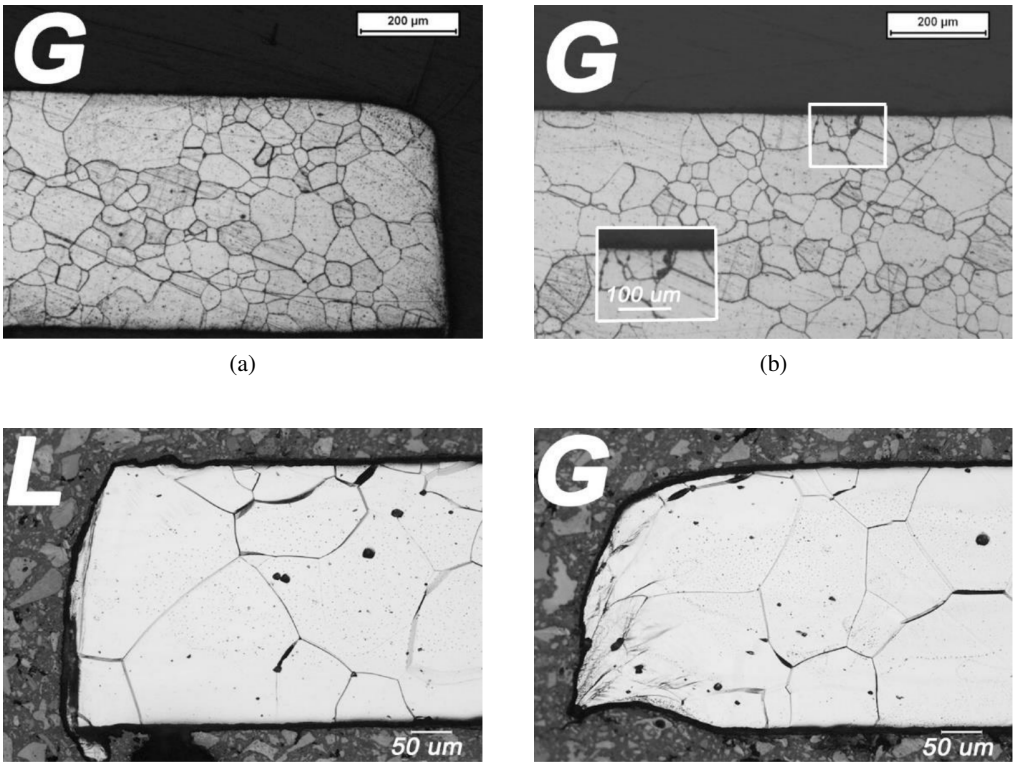

(a) (b)

(c) (d)

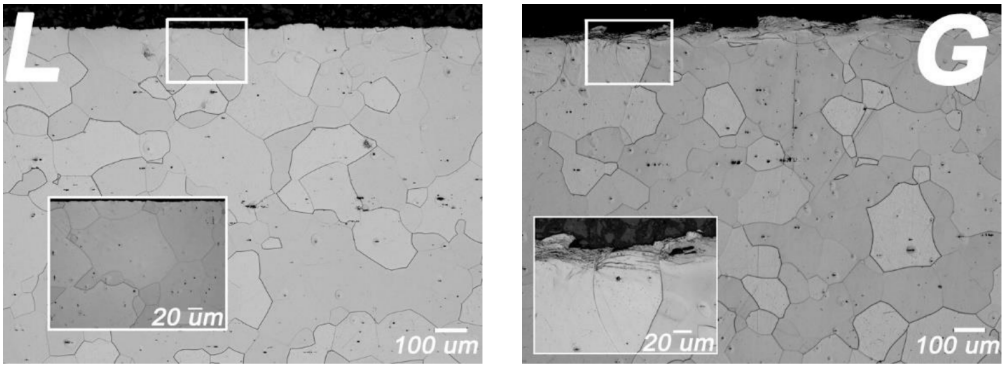

(e) (f)

Fig. 10. Observed material microstructures: M300-35 (c), (f) and M470-50 (a), (b); *G* – guillotine, *L* – laser. The microstructure: in the cross section of the strips (a), (c) and (d); in a plane parallel to the strip surface (b), (e) and (f)

Using the Phenom ProX microscope, it was found that the tested strips had a single-phase microstructure of recrystallized ferrite with different grain sizes. The average grain size was about 150 µm (M300-35) and 70 µm (M300-35). In the M300-35 material, even larger grains covered the entire thickness of the strip were observed. On the other hand, in the M470-50 material, single grains with a size exceeding 200 µm were observed.

In the case of guillotine cutting, the ferrite microstructure underwent strong plastic deformation right at the cut edge. Numerous slip bands were present in the neighboring grains (Fig. 11(a)). Defects in the microstructure of ferrite grains reached up to about 150–200 µm from the cut edge. In the case of laser cutting, the edge of the strip was more regular compared to the edge cut with a guillotine. The cut passed through the grains without deforming them (Fig. 11(b)). Directly at

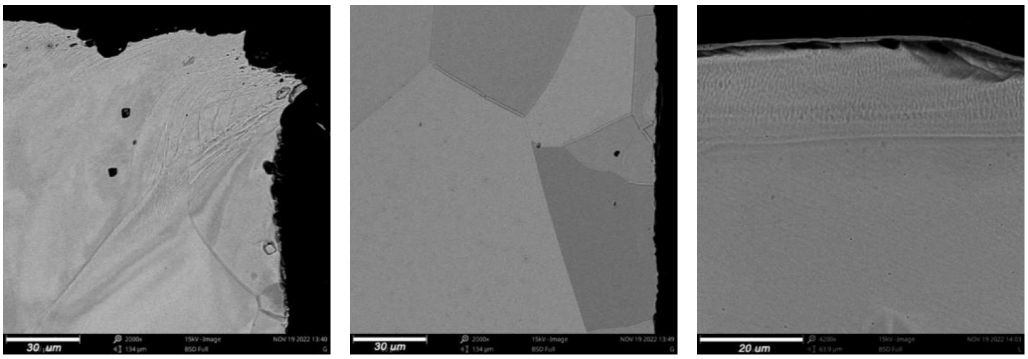

(a) (b) (c)

Fig. 11. The observed microstructure of the strip at the cut edge: (a) guillotine cutting; (b) and (c) laser cutting (M300-35 material)

the edge, a remelted zone with a thickness of 20 µm was observed, with a visible direction of heat dissipation perpendicular to the edge (Fig. 11(c)).

4.4. Measurements of residual stresses in strips

Residual stress tests in the strip made of M300-35 material were carried out using the X-ray $\sin^2\psi$ method based on a Proto Manufacturing Ltd. diffractometer applying $\mathrm{CrK}_\alpha = 0.2291$ nm radiation (V filter). Measurements were made on the reflection (211) ($2\theta = 156.41°$). The tests were carried out on both surfaces of the strips (marked as A and B), and more precisely in the surface layer of the strips to a depth of approx. 16 µm ($G_x = 0.95$ [28]). On the (A) side, measurements were made at points distant from the cut edge by 0.5, 1.5, 2.5 and 10 mm, respectively. On the (B) side, a comparative measurement was made at one point 0.5 mm from the edge – see Fig. 12. The obtained comparative residual stresses, measured at the indicated points of the (B) side were, respectively: –179 MPa for the strip cut with a guillotine and –126 MPa for the strip cut with a laser.

The measurement of residual stresses in materials with relatively large grains poses many difficulties. For this reason, measurements were made using a linear aperture with a beam cross-section of 1×5 mm. As practice has shown, the applied linear aperture, averaging the stress results, turned out to be more useful compared to the point aperture, which is usually used in stress measurements in metals with smaller average grain size [29]. In the case of the tested M300-35 material, the point aperture "generates" results that are very dependent on the selected surface fragment (selected grain). The following X-ray material constants, $1/2S_2 = 6.14 \times 10^{-6}$ 1/MPa and $-S_1 = 1.38 \times 10^{-6}$ 1/MPa, were used in the stress calculation process. The determined residual stresses, obtained by linear aperture, are shown in Fig. 13.

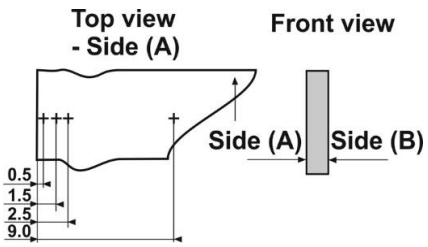

Fig. 12. Location of points on side (A) for measuring residual stresses

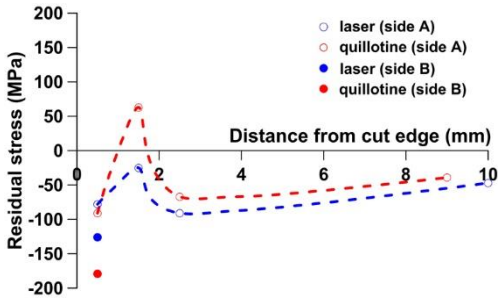

Fig. 13. Measured residual stresses vs. distance from the cut edge (M300-35)

In the middle part of the strip, at a distance of 9–10 mm from the cut edge, the residual stresses had small values of about –40 MPa. As shown in [30], such value of residual stresses occurs in undamaged fragments of the material, as a result of the manufacturing process. At the measurement points located close to the cut edge, the compressive residual stresses had much higher absolute values than those in the central part, i.e. in the range of $-80 \div -180$ MPa (Fig. 13). As a result of the tests, it was found that the residual stresses at the guillotine-cut

edge were higher by 10–70 MPa compared to the stresses at the laser-cut edge. The area of compensation of near-edge stresses was located approx. 1.5 mm from the edge. In the case of the strip cut with a guillotine, the stresses in this area were tensile stresses at a level of 60 MPa, and in the case of the strip cut with a laser they were close to 0.

5. Discussion

The research conducted extends the existing knowledge in the field of modeling the local magnetic permeability of the material. The research conducted by the authors shows that in the case of guillotine and laser cutting, a common formula, (2), can be used successfully. An important modification proposed by the authors is the introduction of a variable width $dd(x)$ to Eq. (2). Moreover, as it was shown in the work, the current value of the $dd(w)$ and $dd(x)$ widths depend on the distance from the cut edge, on the magnetic field strength and cutting technology used (Figs. 7 and 8). This is in line with the results of the research presented in [31]. The proposed analytical model made it possible to plot the curves of local relative magnetic permeability, occurring at a short distance from the edge (Fig. 14). In the case of laser-cut materials, a drastic deterioration of the magnetic properties of the material in the zone showing relatively weak magnetic activity was observed. Its width depends on the strength of the magnetic field and the type of material. For the material cut with a guillotine, such a breakdown of magnetic properties was observed only for magnetic field strengths lower than 100 A/m. For a field strength of 100 A/m, it was respectively: 0.15 mm for the M300-35 material and 0.05 mm for the M470-50 material. The dependence of the width of the magnetically hardened zone (with relatively weak magnetic activity) on the magnetic field strength is shown in Fig. 15. The determined widths are in line with the available results [31].

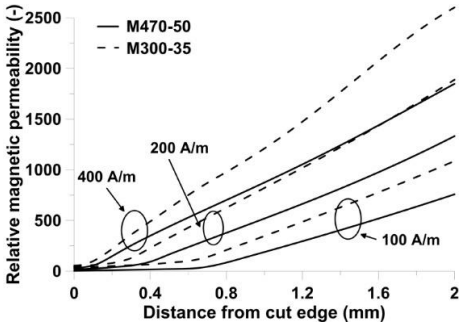

Fig. 14. Local relative magnetic permeability vs. distance from the cut edge

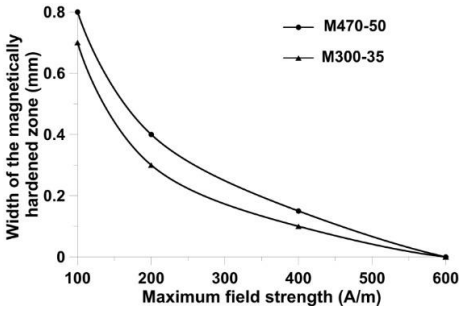

Fig. 15. Width of the magnetically hardened zone vs. maximum field strength

For materials cut with a guillotine, the local magnetic permeability curves shown in Fig. 7 stabilize their value at a distance of about 2 mm (M470-50) and 1.8 mm (M300-35). This distance is consistent with that in which residual stresses are compensated (Fig. 13), and in line with results presented in the literature [14, 26, 27]. At low magnetic field strength, in the case of laser cutting,

the degraded domain structure additionally deteriorates the macroscopic properties. As shown in Fig. 7, the local magnetic permeability curves stabilize their value about 8–9 mm from the edge. The work [13] shows that at low magnetic fields, zones with a relatively weak magnetic activity may occur even at a distance of up to 6–7 mm from the edge. Thus, the results obtained by the authors are in line with the studies of other scientists.

6. Conclusions

The paper describes the results of macroscopic and microscopic studies of low-loss Fe-Si materials. The authors proved that the local material parameters, such as magnetic permeability, can be successfully reconstructed on the basis of macroscopic studies. The work showed that in the case of laser cutting, the influence of magnetic and mechanical hardening of the material at the edge can be effectively modeled. In addition, it has been shown that the dependence of the $dd(x)$ parameter on the distance from the edge and the magnetic field strength allows much more accurate modeling of the local magnetic permeability curves. This is particularly evident for relatively low magnetic field strengths. According to the authors, in order to fully understand the principles of modeling local material properties (especially in the vicinity of the laser-cut edge), further studies with the MOKE microscope are necessary.

Acknowledgements

The authors would like to thank Jacek Szulakowski for his help in carrying out the magnetic measurements.

This research was funded by National Science Centre (NCN) Poland as part of the Opus–18, grant number 2019/35/B/ST8/00764: "*The manufacturing technology impact analysis of small-power high-speed electric motors to refine their analytical models*".

References

[1] Liu H., Lee J., *Optimum design of an IE4 line-start synchronous reluctance motor considering manufacturing process loss effect*, IEEE Transactions on Industrial Electronics, vol. 65, no. 4, pp. 3104–3114 (2018), DOI: 10.1109/TIE.2017.2758738.

[2] De Almeida A.T., Fereira F.J., Baoming G., *Beyond induction motor – Technology trends to move up efficiency*, IEEE Transactions on Industry Applications, vol. 50, no. 3, pp. 2103–2114 (2014), DOI: 10.1109/TIA.2013.2288425.

[3] Dorrell D.G., *The challenges of meeting IE4 efficiency standards for induction and other machines*, Proceedings of IEEE International Conference on Industrial Technology, Busan, South Korea, pp. 213–218 (2014), DOI: 10.1109/ICIT.2014.6894941.

[4] Cavagnino A., Vaschetto S., Ferraris L., Gmyrek Z., Agamloh E., Bramerdorfer G., *Towards an IE4 efficiency class for induction motors with minimal manufacturer impact*, Proceedings of IEEE Energy Conversion Congress and Exposition, Portland, USA, pp. 289–296 (2018), DOI: 10.1109/ECCE.2018.8557586.

[5] Kerdsup B., Kreuawan S., *Design of synchronous reluctance motors with IE4 energy efficiency standard competitive to BLDC motors used for blowers in an conditioners*, Proceedings of IEEE International

Electric Machines and Drives Conference, Miami, USA, pp. 1–6 (2017), DOI: 10.1109/IEMDC.2017.8002025.

[6] Wolnik T., Opach S., Cyganik Ł., Jarek T., Szekeres V., *Design methods for limiting rotor losses in a fractional slot PMSM motor with high power density*, Archives of Electrical Engineering, vol. 71, no. 4, pp. 963–979 (2022), DOI: 10.24425/aee.2022.142119.

[7] Arshad W.M., Ryckebush T., Magnussen F., Lendenmann H., Soulard J., Eriksson B., Malmros B., *Incorporating lamination processing and component manufacturing in electrical machine design tools*, Proceedings of IEEE Industry Applications Annual Meeting, New Orleans, USA, pp. 94–102 (2007), DOI: 10.1109/07IAS.2007.21.

[8] Clerc A.J., Muetze A., *Measurement of stator core magnetic degradation during the manufacturing process*, IEEE Transactions on Industry Applications, vol. 48, no. 4, pp. 1344–1352 (2012), DOI: 10.1109/TIA.2012.2199950.

[9] von Pfingsten G., Steentjes S., Thul A., Herold T., Hameyer K., *Soft magnetic material degradation due to manufacturing process: A comparison of measurements and numerical simulations*, Proceedings of International Conference on Electrical Machines and Systems, Hangzhou, China, pp. 2018–2024 (2014), DOI: 10.1109/ICEMS.2014.7013817.

[10] Bali M., De Gersem H., Muetze A., *Finite-element modeling of magnetic material degradation due to punching*, IEEE Transactions on Magnetics, vol. 50, no. 2, article sequence number 7018404 (2014), DOI: 10.1109/TMAG.2013.2283967.

[11] Shi W., Liu J., Li C., *Effect of cutting techniques on the structure and magnetic properties of a high-grade non-oriented electrical steel*, Journal of Wuhan University of Technology, vol. 29, no. 6, pp. 1246–1251 (2014), DOI: 10.1007/s11595-014-1076-3.

[12] Sundaria R., Nair D.G., Lehikoinen A., Arkkio A., Belahcen A., *Effect of laser cutting on core losses in electrical machines – Measurements and modeling*, IEEE Transactions on Industrial Electronics, vol. 67, no. 9, pp. 7354–7363 (2020), DOI: 10.1109/TIE.2019.2942564.

[13] Saleem A., Alatawneh N., Rahman T., Lowther D.A., Chromik R.R., *Effects of laser cutting on microstructure and magnetic properties of non-orientation electrical steel laminations*, IEEE Transactions on Magnetics, vol. 56, no. 2, 6100609 (2020), DOI: 10.1109/TMAG.2020.3029256.

[14] Bali M., De Gersem H., Muetze A., *Determination of original nondegraded and fully degraded magnetic characteristics of material subjected to laser cutting*, IEEE Transactions on Industry Applications, vol. 53, no. 5, pp. 4242–4251 (2017), DOI: 10.1109/TIA.2017.2696479.

[15] Elfgen S., Steentjes S., Bohmer S., Franck D., Hameyer K., *Influences of material degradation due to laser cutting on the operating behavior of PMSM using a continuous local material model*, IEEE Transactions on Industry Applications, vol. 53, no. 3, pp. 1978–1984 (2017), DOI: 10.1109/TIA.2017.2665338.

[16] Schauerte B., Xiao X., Jansen K., Hameyer K., *Consideration of the spatial orientation of magnetic field quantities and tensile mechanical stress in the Finite Element Analysis of electrical machines*, Archives of Electrical Engineering, vol. 71, no. 4, pp. 949–961 (2022), DOI: 10.24425/aee.2022.142118.

[17] Martin F., Aydin U., Sundaria R., Rasilo P., Belahcen A., Arkkio A., *Effect of punching the electrical sheets on optimal design of a permanent magnet synchronous motor*, IEEE Transactions on Magnetics, vol. 54, iss. 3, article sequence number 8102004 (2018), DOI: 10.1109/TMAG.2017.2768399.

[18] Manescu V., Paltanea G., Ferrara E., Nemoianu I.V., Fiorillo F., Gavrila H., *Influence of mechanical and water-jet cutting on the dynamic magnetic properties of NO Fe-Si steels*, Journal of Magnetism and Magnetic Materials, vol. 499, article sequence number 166257 (2020), DOI: 10.1016/j.jmmm.2019.166257.

[19] Daem A., Sergeant P., Dupre L., Chadhuri S., Bliznuk V., Kestens L., *Magnetic properties of silicon steel after plastic deformation*, Materials, vol. 13, article sequence number 4361 (2020), DOI: 10.3390/ma13194361.

[20] Xie S., Wu L., Tong Z., Chen H., Chen Z., Uchimoto T., Takagi T., *Influence of plastic deformation and fatigue damage on electromagnetic properties of 304 austenic stainless steel*, IEEE Transactions on Magnetics, vol. 54, no. 8, article sequence number 6201710 (2018), DOI: 10.1109/TMAG.2018.2819123.

[21] Cao H., Hao L., Yi J., Zhang X., Luo Z., Chen S., Li R., *The influence of punching process on residual stress and magnetic domain structure of non-oriented silicon steel*, Journal of Magnetism and Magnetic Materials, vol. 406, pp. 42–47 (2016), DOI: 10.1016/j.jmmm.2015.12.098.

[22] Singh D., Rasilo P., Martin F., Belehcen A., Arkkio A., *Effect of mechanical stress on excess loss of electrical steel sheets*, IEEE Transactions on Magnetics, vol. 51, no. 11, article sequence number 1001204 (2015), DOI: 10.1109/TMAG.2015.2449779.

[23] Gurbuz I.T., Martin F., Aydin U., Ali A.B., Chamosa M., Rasilo P., Belahcen A., *Experimental characterization of the effect of uniaxial stress on magnetization and iron losses of electrical steel sheets cut by punching process*, Journal of Magnetism and Magnetic Materials, vol. 549, article sequence number 168983 (2022), DOI: 10.1016/j.jmmm.2021.168983.

[24] Sundaria R., Leihkoinen A., Arkkio A., Hannukainen A., *Higher-order finite element modeling of material degradation due to cutting*, Proceedings of IEEE International Electric Machines and Drives Conference, Miami, USA, pp. 1–7 (2017), DOI: 10.1109/IEMDC.2017.8002278.

[25] Vandenbossche L., Jacobs S., Henrotte F., Hameyer K., *Impact of cut edges on magnetization curves and iron losses in e-machines for automotive traction*, Word Electric Vehicle Journal, vol. 4, no. 1, pp. 587–596 (2010), DOI: 10.3390/wevj4030587.

[26] Gmyrek Z., *Impact of a punching process on the SyRM iron loss: SPICE model as an effective tool for iron loss modeling*, Energies, vol. 14, pp. 1–19 (2021), DOI: 10.3390/en14217185.

[27] Gmyrek Z., Cavagnino A., *Analytical model of the ferromagnetic properties in laminations damaged by cutting*, Proceedings of IEEE Energy Conversion Congress and Exposition, Vancouver, Canada, pp. 4000–4007 (2021), DOI: 10.1109/ECCE47101.2021.9595736.

[28] Kucharska B., *Measurement of Fe-Cr-Ni coatings density in XRD analysis*, Inżynieria Materiałowa – Materials Engineering, vol. 28, no. 3–4, pp. 419–421 (2007).

[29] Kucharska B., Moraczyński O., *Exhaust system piping made by hydroforming: relations between stresses, microstructure, mechanical properties and surface*, Archives of Civil and Mechanical Engineering, vol. 20, no. 141 (2020), DOI: 10.1007/s43452-020-00142-x.

[30] Xiong X., Hu S., Dang N., Hu K., *Effect of stress-relief annealing on microstructure, texture and hysteresis curve of mechanically cut non-oriented Fe-Si steel*, Materials Characterization, vol. 132, pp. 239–247 (2017), DOI: 10.1016/j.matchar.2017.06.035.

[31] Naumoski H., Riedmüller B., Minkow A., Herr U., *Investigation of the influence of different cutting procedures on the global and local magnetic properties of non-oriented electrical steel*, Journal of Magnetism and Magnetic Materials, vol. 392, pp. 126–133 (2015), DOI: 10.1016/j.jmmm.2015.05.031.